Equatorial Waves in a Stratospheric GCM: Effects of Vertical Resolution

BYRON A. BOVILLE AND WILLIAM J. RANDEL

National Center for Atmospheric Research, Boulder, Colorado*

(Manuscript received 17 April 1991, in final form 10 September 1991)

ABSTRACT

Equatorially trapped wave modes, such as Kelvin and mixed Rossby–gravity waves, are believed to play a crucial role in forcing the quasi-biennial oscillation (QBO) of the lower tropical stratosphere. This study examines the ability of a general circulation model (GCM) to simulate these waves and investigates the changes in the wave properties as a function of the vertical resolution of the model. The simulations produce a stratopause-level semiannual oscillation but not a QBO.

An unfortunate property of the equatorially trapped waves is that they tend to have small vertical wavelengths ($\leq$15 km). Some of the waves, believed to be important in forcing the QBO, have wavelengths as short as 4 km. The short vertical wavelengths pose a stringent computational requirement for numerical models whose vertical grid spacing is typically chosen based on the requirements for simulating extratropical Rossby waves (which have much longer vertical wavelengths). This study examines the dependence of the equatorial wave simulation of vertical resolution using three experiments with vertical grid spacings of approximately 2.8, 1.4, and 0.7 km.

Several Kelvin, mixed Rossby–gravity, and inertio–gravity waves are identified in the simulations. At high vertical resolution, the simulated waves are shown to correspond fairly well to the available observations. The properties of the relatively slow (and vertically short) waves believed to play a role in the QBO vary significantly with vertical resolution. Vertical grid spacings of about 1 km or less appear to be required to represent these waves adequately.

The simulated wave amplitudes are at least as large as observed, and the waves are absorbed in the lower stratosphere, as required in order to force the QBO. However, the EP flux divergence associated with the waves is not sufficient to explain the zonal flow accelerations found in the QBO.

1. Introduction

Several general circulation models (GCMs) intended for simulating the middle atmosphere have been constructed in recent years, and results have been reported in the scientific literature (e.g., Mahlman and Umscheid 1984; Boville and Randel 1986; Rind et al. 1988a,b). A notable failure of these GCMs has been their inability to simulate the quasi-biennial oscillation (QBO) of the equatorial lower stratosphere.

The QBO, which dominates the variability of the zonal mean wind in the equatorial lower stratosphere, was discovered independently by Reed et al. (1961) and by Veryard and Ebdon (1961). It consists of alternating regions of easterlies and westerlies that propagate downward over time with a variable period averaging about 26 months. A recent summary of the properties of the QBO is given by Naujokat (1986). A plausible theoretical explanation of the QBO was first proposed by Lindzen and Holton (1968). Holton and Lindzen (1972) proposed a revised form of the theory that is still generally accepted and is summarized briefly below. Numerous one- and two-dimensional simulations of the QBO have been published using models based on the Holton–Lindzen theory (e.g., Dunkerton 1981; Takahashi 1987). A QBO-like phenomenon has even been produced in a laboratory experiment by Plumb and Bell (1982). However, no GCM simulations of the QBO have ever been reported. Indeed, no three-dimensional numerical QBO simulations of any kind were reported prior to the work of Takahashi and Boville (1992) using a simplified "mechanistic" model.

Figure 1 shows what seems to be a fairly typical simulation of the time evolution of the equatorial zonal wind from GCM simulations. The experiment from which the results were obtained is described below. A semiannual oscillation (SAO) can be seen in Fig. 1 in the vicinity of the stratopause (near 1 mb) and in the vicinity of the tropopause (near 100 mb). Reasonably successful simulations of the stratopause SAO have previously been reported by Hamilton and Mahlman (1988) and by Rind et al. (1988b). In common with those studies, Fig. 1 shows no evidence of a QBO in the region between 100 and 5 mb.

* The National Center for Atmospheric Research is sponsored by the National Science Foundation.

Corresponding author address: Dr. Byron A. Boville, National Center for Atmospheric Research, Climate and Global Dynamics Division, P.O. Box 3000, Boulder, CO 80307-3000.

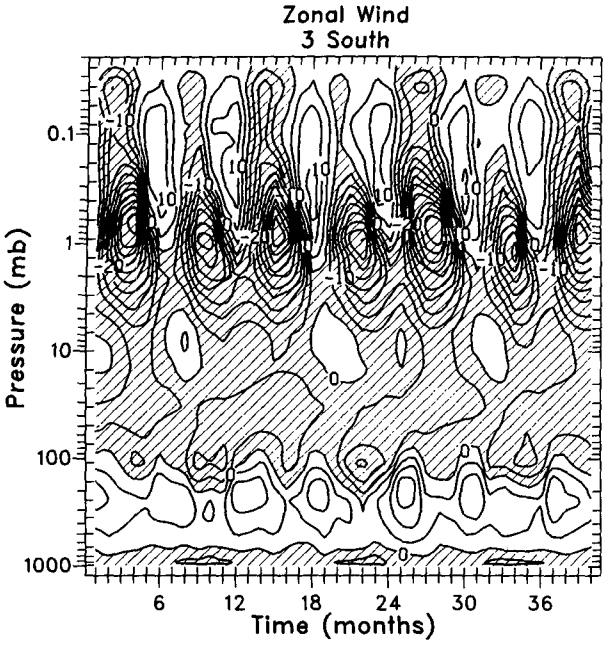

FIG. 1. Time–height cross section of the monthly and zonally averaged zonal wind at 3°S for L30. Month 1 is November. The contour interval is 5 m s^{-1}; regions with negative values are hatched.

The Holton–Lindzen theory of the QBO is based on the interaction of two equatorially trapped wave modes with the background (zonal mean) flow. The easterlies are believed to be forced by westward-propagating (easterly phase speed) mixed Rossby–gravity (MRG) waves with zonal wavenumber 4 or 5 and periods near 5 days. The westerlies are believed to be forced by eastward-propagating Kelvin waves with zonal wavenumber 1 and periods near 15 days. The existence of these waves in the equatorial lower stratosphere was first reported by Yanai and Maruyama (1966) and by Wallace and Kousky (1968). Both waves decay exponentially away from the equator, with meridional scales of about 10 degrees. The vertical scales of the observed waves fit with the expected structure of Kelvin and MRG waves. Their vertical wavelengths are ~5–10 km away from critical levels (where the wave phase speed equals the zonal wind speed) and decrease rapidly as the waves approach critical levels.

GCMs are computationally expensive and have strong constraints on the resolution that can be used, especially when multiyear simulations are required. Horizontal resolutions have typically been restricted to 2.5° or greater, resulting in models that are capable of representing horizontal wavelengths greater than ~1000 km, since at least four grid points are required to represent a wave accurately. The prime concern in most middle-atmosphere GCM studies has been on extratropical circulations, where quasigeostrophic dynamics impose the relationship $L_h/L_z = N/f \sim 100$ (where N is the Brunt–Väisälä frequency and f is the Coriolis parameter) between the horizontal and vertical length scales of disturbances. Therefore, the vertical resolution in current middle atmosphere GCMs is usually chosen to be roughly consistent with the horizontal resolution using the above scaling relationship (this choice has not always been deliberate). Given ~1000-km minimum horizontal wavelengths, vertical resolutions have been restricted to ~2.5 km or greater in order to resolve vertical wavelengths longer than ~10 km.

Designing GCMs for extratropical problems has resulted in models that are not capable of properly resolving the waves believed to be important in forcing the QBO. Far from critical levels, the Kelvin waves can be resolved by some GCMs, but the MRG waves cannot. As critical levels are approached, even the Kelvin waves rapidly become too short to be resolved. This point has been made previously by Plumb (1984), among others. Experience with idealized one- and two-dimensional models (Takahashi, personal communication) has indicated that QBO simulations are possible with a vertical resolution of 1 km or smaller but that no QBO occurs at resolutions as coarse as 2 km. This constraint is probably based on simulating the sharp shear zones in the zonal mean flow. The idealized models do not even attempt an explicit representation of the waves, as in a GCM, but use the WKB approximation to solve directly for the wave momentum flux based on the mean state.

Takahashi and Boville (1992) have simulated the QBO by running a simplified three-dimensional model at very high vertical resolution (1/2-km vertical grid spacing). The model was simplified by eliminating the troposphere and directly forcing Kelvin and MRG waves at the tropical tropopause instead of relying on a GCM's tropospheric simulation to produce them. The present study examines the behavior of equatorial waves in a full GCM as the vertical resolution is increased to the point of being adequate to resolve them.

Distinct Kelvin and MRG modes are readily identifiable in both the model and observations. We examine the amplitudes, structures, and mean flow forcing for several waves, including those associated with the QBO in the Holton–Lindzen theory. It is instructive to examine individual modes because the analysis of both model and observations shows that the wave variance is concentrated along modal dispersion curves (associated with preferred vertical wavelengths). It should be noted that the particular zonal wavenumbers and frequencies typically associated with the QBO contribute only ~10% of the total mean flow forcing. This occurs because variance is distributed at multiple zonal wavenumbers along dispersion curves and because multiple modes are present.

The GCM, the experiments, and the analysis methods are described in section 2. The Kelvin waves produced by the model and their variation with resolution

TABLE 1. List of experiments.

Name	Number of levels	Max spacing $\Delta \ln(p)$	Max spacing height (km)	Length (months)
L30	30	0.4	2.8	40
L55	55	0.2	1.4	5
L107	107	0.1	0.7	5

are discussed in section 3 and MRG waves are discussed in section 4. Conclusions appear in section 5.

2. Model description and analysis methods

The model used in this study is based on the NCAR Community Climate Model, Version 1 (CCM1; Williamson et al. 1987), where the parameterizations of convection, surface processes, vertical diffusion, and radiative transfer are described. The original model was intended for the simulation of the troposphere, and extensive modifications have been incorporated in the process of extending the model domain vertically to include the upper stratosphere and lower mesosphere as described in Boville and Baumhefner (1990). The modifications include the use of a hybrid vertical coordinate following Simmons and Strüfing (1983) that reduces to pressure above 100 mb and the use of biharmonic horizontal diffusion at all levels. The model uses the spectral transform method in the horizontal, with the spherical harmonic expansions truncated at total wavenumber 21 (T21).

The experiments in this study used a vertical domain extending from the surface to 0.025 mb (~75 km) and employed 30, 55, or 107 levels. The standard version of CCM1 uses 12 levels spaced relatively close together [in $\ln(p)$, or height] near the surface. The [$\ln(p)$] distance between adjacent levels increases monotonically away from the surface and exceeds 0.4-scale heights above 110 mb. The 30-level model maintains a constant spacing of 0.4-scale heights (about 2.8 km) above 110 mb, consistent with a horizontal resolution of about T42 (~1000-km minimum resolved scale). The 55- and 107-level models were constructed by decreasing the maximum spacing between levels to 0.2- and 0.1-scale heights, respectively. In each case, the original CCM1 levels were used until their spacing exceeded the specified threshold. Above this point, the levels were equally spaced in $\ln(p)$. The level spacings are summarized in Table 1.

All of the experiments begin on 15 October using initial conditions from a previous simulation, and the subsequent analysis of equatorial wave properties uses the 120-day period from 15 November to 15 March (only the first year is used from the 40-month L30 run).

Figure 1 shows the time evolution of the equatorial zonal mean wind for L30. As mentioned above, an SAO is evident at the stratopause but there is no evidence of a QBO. The results of Takahashi and Boville (1992) indicate that whether a QBO will occur in a simulation should be obvious within the first 40 months. Of course, a QBO is not expected in the L30 simulation because of the 2.8-km vertical grid spacing.

Figure 2 shows the zonal mean winds in the tropics averaged over the 4-month analysis period for all three experiments. The three simulations are similar in the tropics, although there is a systematic strengthening of the easterlies in the upper stratosphere and lower mesosphere as the resolution increases. The westerly shear zone over the equator between 1 and 0.1 mb strengthens considerably as the resolution increases. L107 is much more realistic than the lower-resolution simulations when compared to the observations for 1979 discussed by Hitchman and Leovy (1986). However, the observational results of Belmont et al. (1975) and Delisi and Dunkerton (1988) indicate that the shears were anomalously strong in 1979. The three simulations are almost identical outside of the tropics, as expected from the quasigeostrophic nature of the dynamics there. The L30 model already has more than enough vertical resolution to be compatible with the T21 truncation.

The power spectra that appear below were obtained by taking the direct Fourier transform of the model fields: first in longitude, then in time. The longitudinal transforms were truncated at (zonal) wavenumber 12. The time transforms are based on 240 time samples (120 days sampled twice daily) giving a Nyquist frequency of 1 day^{-1} (all frequencies are given here in cycles per day). Gaussian smoothing was applied to the spectra before plotting, as in Randel et al. (1990). Wave amplitudes and phases are calculated by integrating the Fourier coefficients over a frequency band for a fixed zonal wavenumber and computing the magnitude and phase (relative to a base point) of the re-

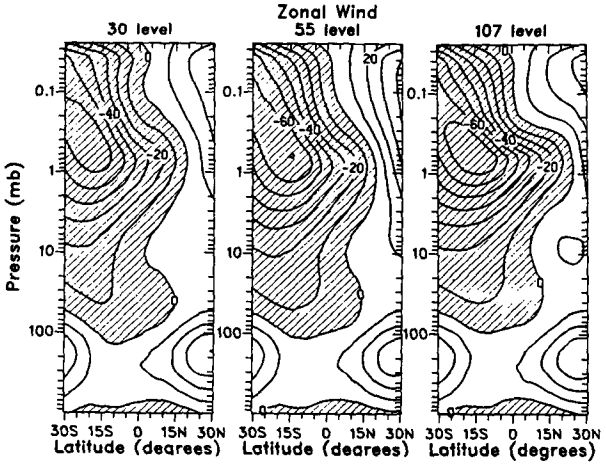

FIG. 2. Latitude–height cross sections of the zonally averaged zonal wind at 3°S for L30, L55, and L107. The contour interval is 10 m s^{-1}; regions with negative values are hatched.

sulting complex coefficient. Coherence with respect to the base point is calculated from the copower and quadpower, and the number of degrees of freedom is estimated as the number of frequencies entering the integral. Significance can then be computed and contours are only plotted where 90% confidence is exceeded. Comparisons of the wave amplitudes with atmospheric observations are made using data from the Limb Infrared Monitor of the Stratosphere (LIMS) instrument on *Nimbus 7* described by Gille and Russell (1984). LIMS version 4 daily data were used for the period 16 November 1978–15 March 1979.

Spectra of the Eliassen–Palm (EP) flux and its divergence (actually the body force per unit mass in the zonal momentum equation) are computed using Eqs. (A1) and (A2) of Dunkerton et al. (1981). Cross-spectral power is substituted for the eddy fluxes resulting in spectra of the EP flux and its divergence. The time and zonal means of the potential temperature and zonal wind are used in place of the zonal means in the original equations.

3. Kelvin waves

Kelvin waves have been identified in LIMS satellite temperature by Salby et al. (1984), among others, and in GCM simulations by Hayashi et al. (1984) and Boville and Cheng (1988). Kelvin waves have several interesting properties that make them easy to identify. They are eastward propagating with equatorially symmetric temperature (Fig. 3) and zonal wind perturbations but negligible meridional wind perturbations.

a. Identification of wave modes

The latitudinal distribution of the L107 temperature spectrum for the lower stratosphere in Fig. 3 is dominated by stationary power outside of the tropics and by an equatorially symmetric eastward-moving feature with period near 15 days (or frequency near 0.067 cycles day^{-1}). The feature decays away from the equator with an e-folding width of $\sim 15°$, in accordance with the latitudinal structure equation for a Kelvin wave of 15-day period and zonal wavenumber one [see Andrews et al. (1987), Eq. (4.7.9)]. This feature in the model's spectrum is associated with the Kelvin wave originally identified in observations by Wallace and Kousky (1968) and believed to be important in forcing the QBO. Wind spectra are not shown; however, the zonal wind has a corresponding symmetric peak. A peak is also found in the meridional wind but is several orders of magnitude smaller than the zonal wind peak, lending further support to the identification of this feature as representing a Kelvin wave.

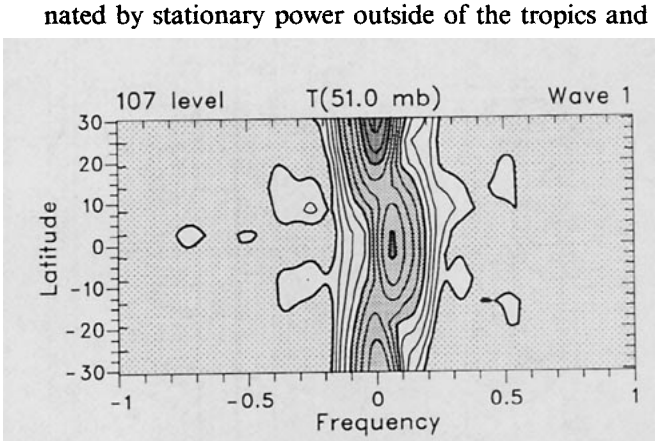

FIG. 3. Frequency–latitude cross section of the $\tilde{k} = 1$ temperature power spectral density (K^2 day) near the 50-mb level for L107. The frequency axis is labeled in cycles per day. Contours are spaced logarithmically with four contours per decade. Light stippling indicates values less than the minimum contour level of 10^{-3}. Medium and heavy stippling indicate values greater than 10^{-2} and 10^{-1}, respectively.

The vertical wavelength of the Kelvin waves observed in the stratosphere is believed to be determined by the vertical structure of the diabatic heating in the troposphere (e.g., Salby and Garcia 1987). The zonal wavenumber spectrum is then determined by the spatial scale of the heating, and the frequency spectrum is determined by the dispersion relation [Andrews et al. (1987), Eq. (4.7.8a)]:

$$\omega = -Nk/m, \qquad (1)$$

where ω is frequency (radians s^{-1}); N is the Brunt–Väisälä frequency; $k = \tilde{k}/a$ and $m = 2\pi/L$ are dimensional zonal and vertical wavenumbers, respectively; $\tilde{k}$ is the nondimensional zonal wavenumber; a is the radius of the earth; and L is the vertical wavelength. All frequencies quoted here are in cycles per day, or $\tilde{\omega} = \omega \times 86\,400/2\pi$. The dispersion relation (1) is valid for weak background winds. The resulting waves are horizontally nondispersive and appear as straight lines emanating from the origin on wavenumber–frequency diagrams (Figs. 4 and 5).

The wavenumber–frequency distributions of temperature power in lower stratosphere for the three resolutions (Fig. 4) are similar, particularly for L107 and L55. Almost all significant power is eastward moving with wavenumbers and frequencies consistent with those of Kelvin waves having vertical wavelengths between 5 and 20 km. L30 also has substantial stationary power because the 50-mb level in L30 is only one level above the tropical tropopause. The tropical troposphere is dominated by stationary power that decays rapidly above the tropopause (see Fig. 5) and is significant only in the first level or two above the tropopause.

According to (1), if the 15-day, $\tilde{k} = 1$ feature in Fig. 3 was a Kelvin wave, it should have $L \approx 10$ km. Indeed, for low wavenumbers the spectrum in Fig. 4 peaks along the $L = 10$ km dispersion line, and this is the strongest feature in the entire wavenumber–frequency spectrum for the lower stratosphere. $L = 10$ corresponds to about four grid lengths in L30, which is rather short to be accurately represented by the vertical finite differences. As might be expected, this wave is weaker

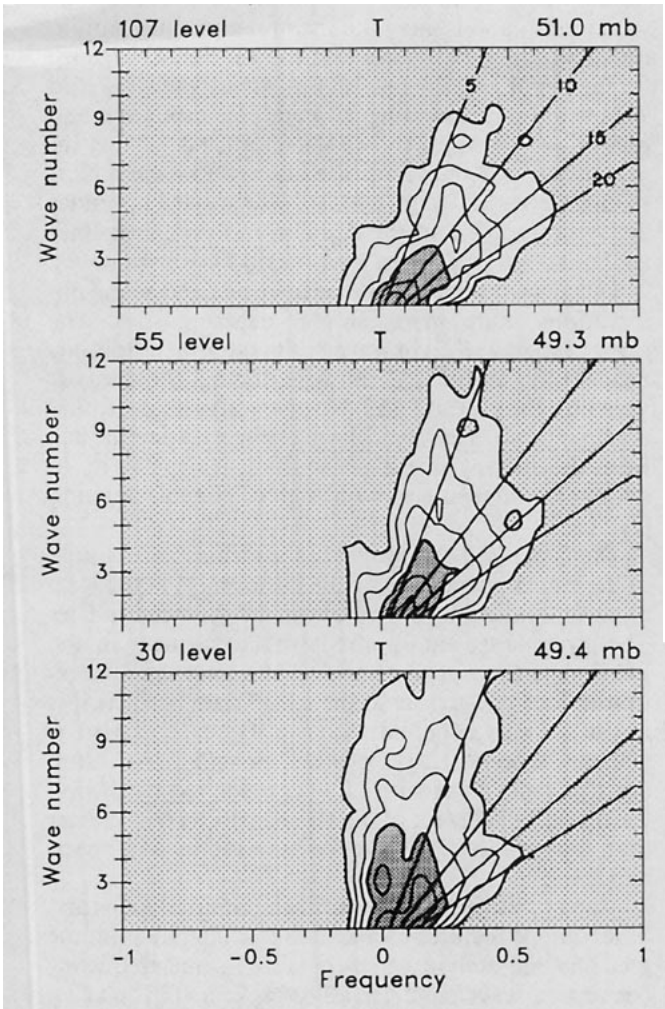

FIG. 4. Frequency–wavenumber cross sections of the temperature power averaged from 10°S to 10°N at the level nearest 50 mb for L107, L55, and L30. Three contours per decade and stippling as in Fig. 3. Dispersion curves are shown for Kelvin waves with L = 5, 10, 15, and 20 km.

in L30 than in the higher resolution simulations; L55 and L107 probably represent this wave fairly well.

Both L30 and L55 have additional spectral peaks at high zonal wavenumber (5–10) and low frequency that lie roughly along the respective dispersion lines for two gridlength waves. These peaks are probably caused by waves that are forced in the lower troposphere, where the resolution is higher in all simulations, and that are misrepresented by the numerics as the levels spread farther apart in the upper troposphere and lower stratosphere. L105 has near uniform resolution above the boundary layer and has noticeably less power at these wavenumbers and frequencies.

The dominant zonal wavenumber and frequency for Kelvin waves tends to shift with height because the vertical group velocity [Andrews et al. (1987), Eq. (4.7.8b)]:

$$c_g^{(z)} = Nk/m^2 = \omega^2/Nk, \qquad (2)$$

depends strongly on these wave properties. The waves are damped as they propagate vertically (largely by radiation) so that power tends to shift toward waves with larger vertical group velocity with height. The wavenumber–frequency spectrum changes with height in two different ways, according to the alternate forms of (2) above. The first form of (2) implies that $c_g^{(z)}$ increases with k along a particular dispersion line (i.e., for fixed L or m). Therefore, the wavenumber–frequency spectrum tends to shift outward along dispersion curves toward larger k with height. The second form of (2) implies that $c_g^{(z)}$ increases with ω for fixed k or that power will tend to shift toward higher frequency with height. Because Kelvin wave packets generally occur at a set of distinct vertical wavelengths, selective damping of the shorter (slower) waves results in the maximum power shifting to dispersion lines of larger L as the height increases. This effect is strengthened by the increase of the radiative damping rate with decreasing L (e.g., Fels 1982), which corresponds to decreasing ω according to (1).

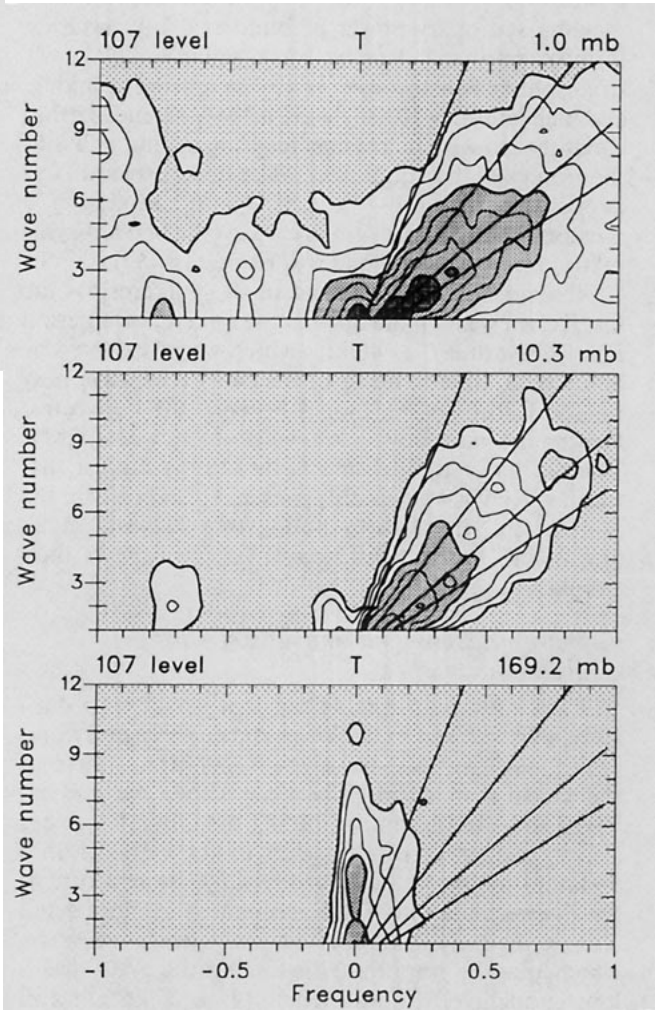

FIG. 5. As in Fig. 4, except that temperature power is shown for L107 near 1, 10, and 170 mb.

Both shifts of the wavenumber–frequency spectrum with height can be seen in Figs. 4 and 5. There is no evidence of Kelvin wave activity below the tropopause (169 mb), where the spectrum is dominated by stationary power. At 50 mb, the spectrum is dominated by the 15-day Kelvin wave with $L \approx 10$ km and $\tilde{k} = 1 \leq 3$, as discussed above. At 10 mb, there is power aligned along two dispersion lines. The power along the $L \approx 10$ km dispersion line has increased for larger k, with significant power at least to $\tilde{k} = 5$, while the power has decreased for small k. The maximum power at 10 mb is still at $\tilde{k} = 1$, but has shifted to $\tilde{\omega} \approx 0.12$ (period near 8.5 days) with power extending along the $L \approx 17$ km dispersion line. At 1 mb, the dominant wave is slightly faster yet, with $\tilde{\omega} \approx 0.133$ (period near 7.5 days) for $\tilde{k} = 1$, and extends along the $L \approx 20$ km dispersion line. Significant eastward power is found near the $L \approx 20$ km dispersion line out to the Nyquist frequency. The westward power at high wavenumbers near the Nyquist frequency at 1 mb probably results from aliasing of even faster eastward power.

Some stationary power is found at 1 mb resulting from extratropical Rossby wave activity. The lower stratospheric Rossby wave activity is confined to middle and high latitudes. Rossby wave activity extends farther equatorward with increasing height, reaching well into the tropics at the stratopause. The fast westward (frequency 0.75) wave 1–2 peak at 10 and 1 mb in Fig. 5 is caused by an inertio–gravity wave (the first antisymmetric mode). This mode will be discussed further.

No evidence can be found in these figures for the fast Kelvin wave in the upper stratosphere, with period near 4 days and $L \approx 40$ km, which was discovered by Salby et al. (1984) using LIMS data. This wave may not be forced in the model because the convective heating is too shallow, a known problem with CCM1. The results of Randel and Gille (1991) suggest that this fast Kelvin wave is only present episodically in the atmosphere. It is worth noting that Hayashi et al. (1984) did find a fast (5-day) Kelvin wave in their simulation.

b. *Wave structures and comparison with observations*

It has now been established that slow ($\sim$15 day) Kelvin waves exist in the lower stratosphere and faster ($\sim$7.5 day) waves exist in the upper stratosphere of the model simulations. The slow Kelvin wave is believed to be important in forcing the QBO, but it has a short enough vertical wavelength ($L \approx 10$ km) that it should not be well resolved by L30. Its structure in the three simulations will be compared in more detail and verified against observations. The faster wave, which may be important in forcing the SAO, has a long enough vertical wavelength ($L \approx 20$ km) that all of the simulations resolve it reasonably well and only L107 will be examined and compared against observations.

Figures 6 and 8 show the mean temperature amplitude and phase structures and the EP flux divergence for the simulated 15- and 7.5-day waves. Figures 7 and 9 show the corresponding temperature amplitudes and phases determined from LIMS data. The EP flux divergence is not shown for the observations because it requires a vertical velocity field. The wave amplitudes are symmetric about the equator and the phase lines are horizontal in all cases, as expected for Kelvin waves.

The Kelvin waves in the simulations and in the observations share many similar characteristics. The slower (15 day) Kelvin wave has maximum amplitude near 40 mb and decays above, although the decay is very slow for L30 and L55. No coherent signal is found above $\sim$5 mb. The vertical wavelength, as determined from the spacing of the phase lines, is 11–12 km, in reasonable agreement with the dispersion relation [Eq. (1)].

The faster (7.5 day) wave has maximum amplitude in the stratosphere near 2 mb, a minimum at the stratopause, and a larger maximum in the mesosphere. The stratopause minimum is much stronger in the LIMS data than in the model. The mesospheric maximum does not appear in the LIMS data because it is not sufficiently coherent with the 10-mb level used as a reference point. The vertical wavelength is 20–21 km, again in agreement with (1). As predicted by theory, the meridional extent of the fast Kelvin wave is greater than that of the slow wave for both model and observations.

Many of the similarities between the simulations and observations mentioned above follow directly from the fact that the Kelvin waves have the same frequency (or vertical wavelength) in all cases. From (1) and (2), once k and either ω or L are specified, then all properties of a Kelvin wave are known, except the amplitude as a function of height. The fact that the frequencies are similar in the CCM and in LIMS data suggests that the vertical scale of the forcing in the model is not much different than that in the atmosphere.

Although the slow Kelvin wave is coherent over approximately the same vertical domain in all three simulations, there is considerable increase of the amplitude with vertical resolution. The maximum amplitude for L107 ($\sim$1.4 K) is nearly twice that for L30, yet even L30 amplitude is somewhat larger than the 0.6 K amplitude of the wave in LIMS data. It should be noted that Wallace and Kousky (1968) quote an amplitude of 2–3 K for this wave. The LIMS data may be underestimating the wave amplitude because the instrument has only $\sim$70% response for waves with $L \approx 10$ km (see Gille and Russell 1984; Gille et al. 1984).

c. *Wave forcing of mean flow*

The observed QBO period is about 26 months (780 days) and the peak-to-peak zonal wind variations are about 40 m s^{-1} (over one-half period), implying that the average acceleration of the zonal wind is roughly

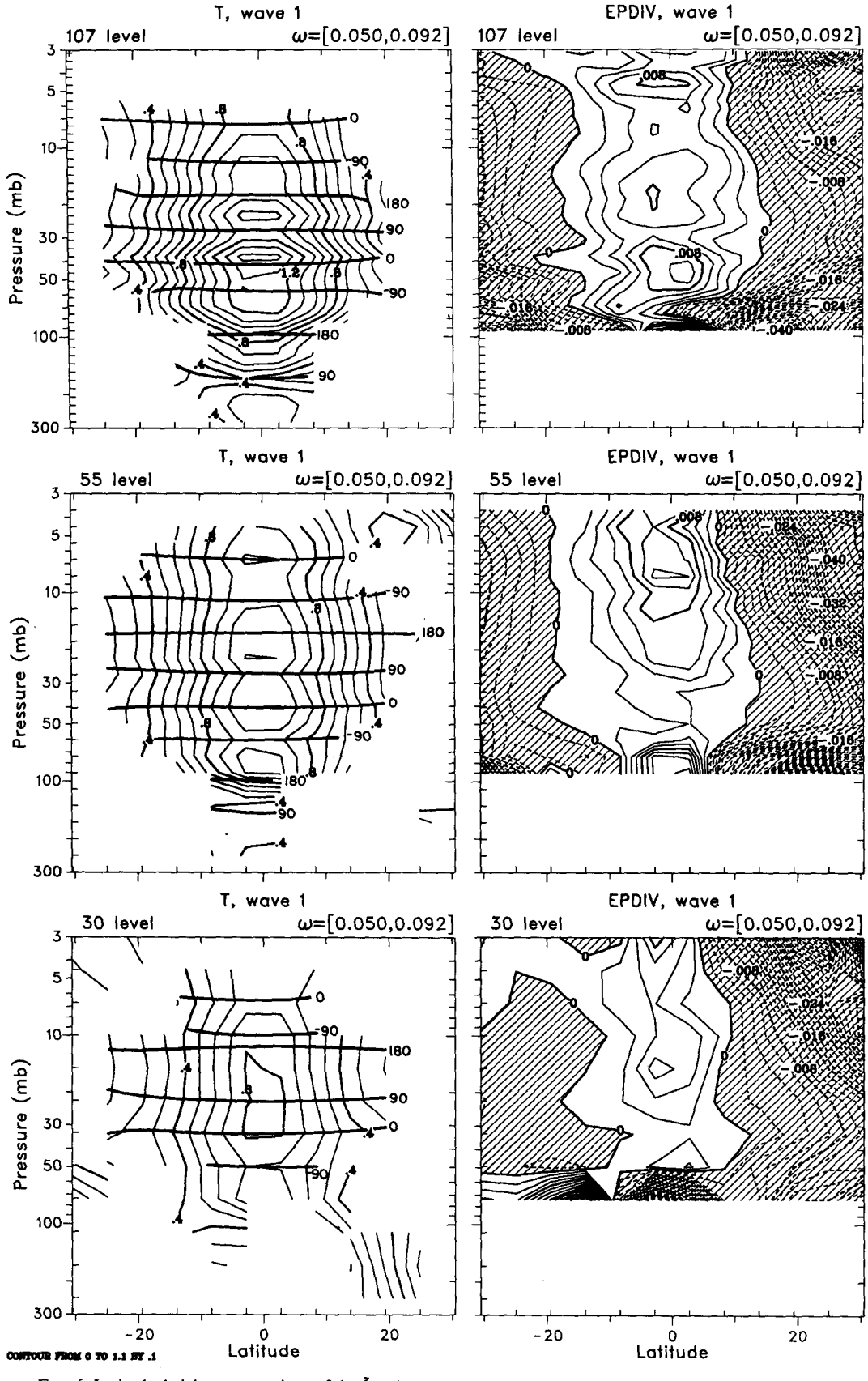

FIG. 6. Latitude–height cross sections of the $\tilde{k} = 1$ temperature amplitude and phase (left) and EP flux divergence (right) for L107 (top), L55 (middle), and L30 (bottom) averaged over a frequency band whose center corresponds to a period of 15 days. The phase is shown relative to a reference point at 40 mb and 2.2°S. The contour interval for temperature is 0.1 K and for EP flux divergence is 2×10^{-3} m s^{-1}/day. Temperature data is contoured only for regions where the significance exceeds 90%.

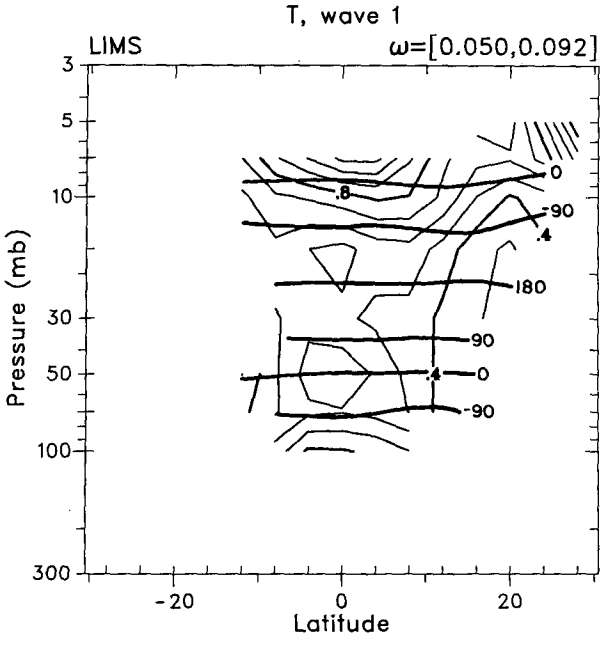

FIG. 7. As in Fig. 6, except that LIMS data are shown for temperature only. The reference point for phase is at 50 mb.

0.1 m s^{-1}/day. The EP flux divergences in Fig. 6 are a measure of the forcing of the mean zonal flow by the waves, although the mean flow accelerations found in the model are usually much smaller than the EP flux divergence, in part because of cancellation with other waves. The maximum EP flux divergence of ~0.01 m s^{-1}/day occurred in L107 in association with a temperature amplitude of ~1.4 K. The EP flux is related to the covariances of wave properties and, therefore, to the square of the wave amplitude. It appears that an amplitude >4 K would be required to produce EP flux divergences of ~0.1 m s^{-1}/day. Even allowing for the effect of the instrument response, the mean wave amplitude during the LIMS observation period was no larger than 1 K, although temperature fluctuations with amplitudes as large as 2 K were routinely present, in agreement with Wallace and Kousky (1968). Therefore, it appears that the slow Kelvin wave present in the model cannot simultaneously reproduce both the observed QBO accelerations and the observed Kelvin wave amplitude.

The variation of the simulated EP flux divergence with vertical resolution for the slow Kelvin is even greater than the variation of the amplitude, as expected from dependence of the EP flux on square of the amplitude. The maximum EP flux divergence occurs lower in the stratosphere as the vertical resolution increases and also increases in magnitude because the wave amplitude increases. From these simulations, it is not possible to draw firm conclusions as to whether the EP flux divergence for the slow Kelvin wave would continue to change significantly with increasing resolution beyond that of L107. However, the fast Kelvin wave can be used to gain more information on this point since its vertical wavelength is twice that of the slow Kelvin wave. Figure 8 shows results only for L107; however, there is little difference between L55 and L107, even in the EP flux divergence. Significant dif-

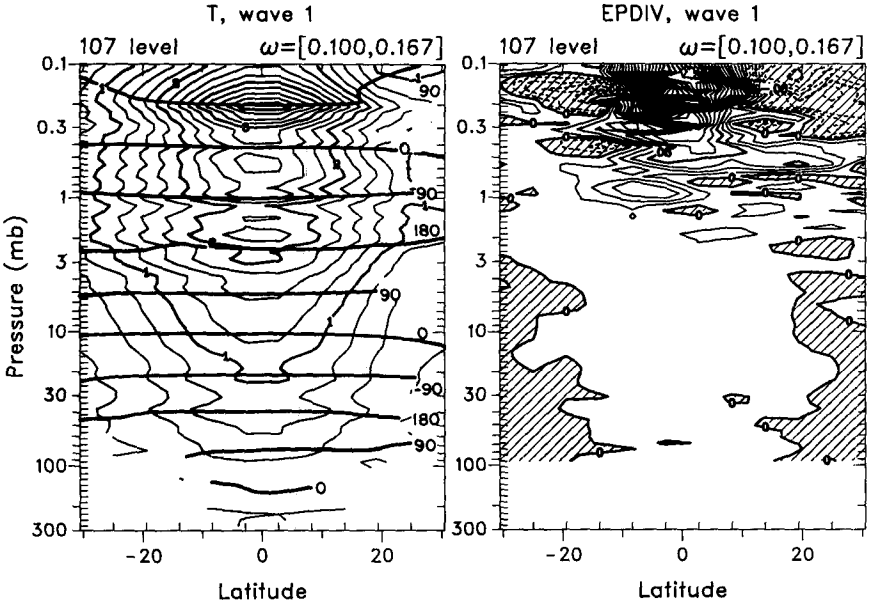

FIG. 8. As in Fig. 6, except that only L107 data are shown. The center of the frequency band corresponds to a period of 7.5 days, the reference point for phase is at 10 mb and 2.2°S, and the contour intervals are 0.25 K for temperature and 2 × 10^{-2} m s^{-1}/day for EP flux divergence.

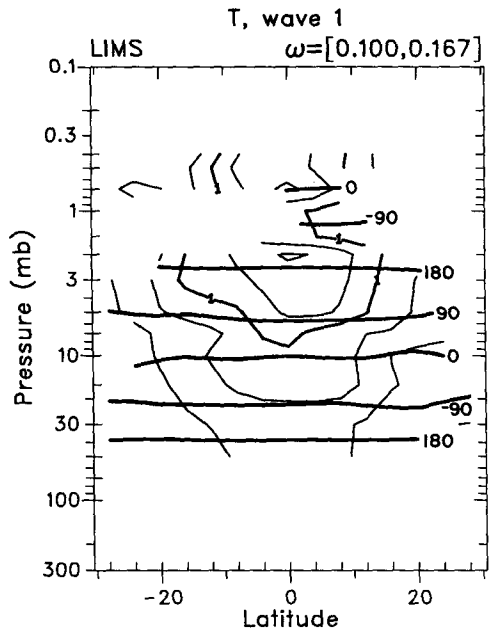

FIG. 9. As in Fig. 8, except that LIMS data are shown for temperature only.

ferences still exist between L30 and L55, although these are less than the differences found for the slower wave. The fast Kelvin wave simulation appears to be roughly invariant to resolution for grid spacings shorter than the ~1.4-km spacing of L55, suggesting that the slower wave is probably invariant to resolution for spacings shorter than the ~700-m spacing of L107. In fact, a grid spacing of about 1 km is probably adequate.

Another aspect of the faster Kelvin wave that is worth mentioning is that it generates EP flux divergence near the stratopause and in the lower mesosphere. This wave (including the $\tilde{k} = 2$, 3 components with the same L) appears to be responsible for at least the bulk of the westerly accelerations in the simulated SAO. Unfortunately, the 120-day period used for the space–time analysis above covers a substantial part of an SAO period that results in smearing the wave forcing in the vertical and making its amplitude appear small. L30 is the only simulation that extends far enough into spring to see the westerlies descend to stratopause level. Therefore, Fig. 10 shows the evolution of the zonal wind, the observed acceleration, and the EP flux divergence associated with wavenumbers 1–6 for L30. The wave forcing is clearly associated with the westerly accelerations of the zonal mean wind and is generally larger than the observed acceleration. This implies that the Kelvin waves (or at least large-scale waves) can explain the westerly phase of the simulated SAO. In contrast, Hamilton and Mahlman (1988) found that gravity waves were largely responsible for forcing the SAO in their simulations.

4. Mixed Rossby-gravity waves

Theory indicates that MRG waves may be either eastward or westward propagating, although the dispersion properties differ depending on the direction of propagation. The 5-day, $\tilde{k} = 4$ westward-propagating

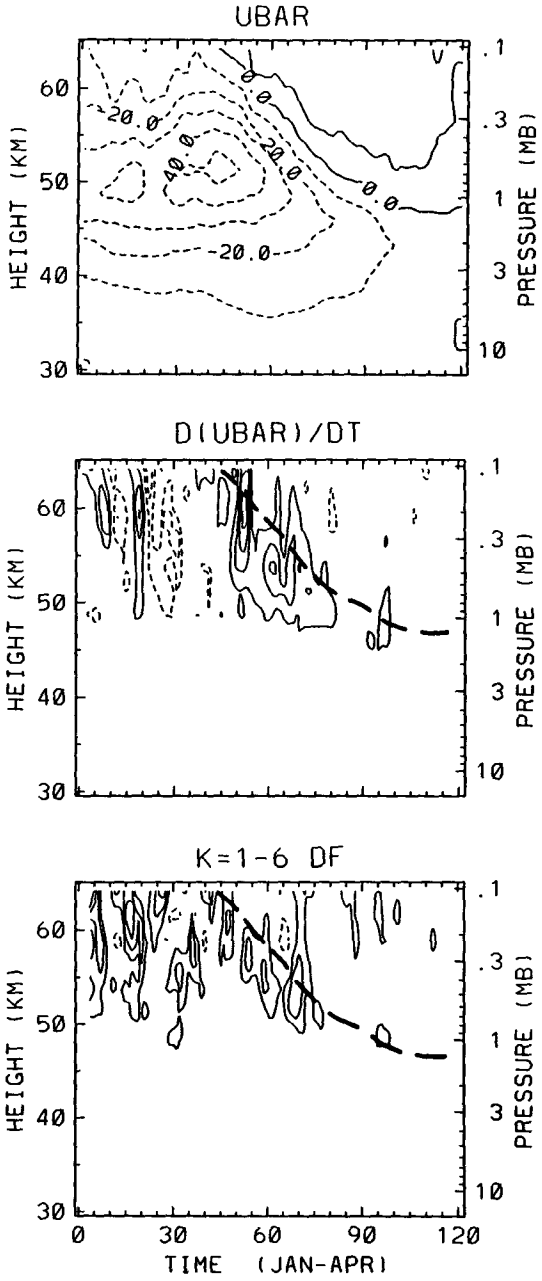

FIG. 10. Time–height cross sections, averaged from 2.8°S to 2.8°N, of the zonally averaged zonal wind (top, contour interval 10 m s^{-1}), its partial derivative with respect to time (middle, contour interval 1 m s^{-1}/day), and the EP flux divergence summed over all frequencies and zonal wavenumbers 1–6 (bottom, contour interval 2 m s^{-1} day^{-1}). Negative contours are dashed. The zero contours are omitted in the lower two panels, and the zero zonal wind line is indicated by a heavy line.

MRG waves, which were discovered by Yanai and Maruyama (1966) using equatorial rawindsonde data, are believed to be important in forcing the QBO. Eastward-propagating MRG waves have rarely been discussed in the literature, although Randel et al. (1990) have identified fast eastward planetary-scale MRG waves using satellite observations together with the model results discussed below.

MRG waves have equatorially symmetric meridional wind perturbations and antisymmetric temperature and zonal wind perturbations. The temperature perturbations are an order of magnitude smaller than those of Kelvin waves, making them more difficult to identify in satellite data. This problem is exacerbated by short vertical wavelengths ($L \leq 8$ km). The response of the LIMS instrument to waves this short is less than 50% (and decreasing rapidly as the wavelength decreases), while most other satellite instruments cannot resolve such wavelengths at all. MRG waves are most easily identified in both rawinsonde data and model output using their meridional wind perturbations, since the other significant equatorial waves (Kelvin waves) have no significant signal in this field. The analysis of MRG waves in model results presents no difficulties since the meridional wind fields are available and can be treated in the same fashion as the temperature fields were treated for analyzing Kelvin waves.

a. *Identification of wave modes*

Following Andrews et al. (1987), the MRG wave dispersion relation can be obtained in a similar form to (1) as

$$\omega = \frac{1}{2m}\{Nk \pm [N^2k^2 + 4mN\beta]^{1/2}\}, \qquad (3)$$

where $\beta = 2\Omega/a$ and Ω and a are the angular velocity and radius of the earth. Dispersion curves are indicated in Fig. 11 for several vertical wavelengths. The plus sign in (3) applies for eastward-propagating waves ($\omega > 0$), and the dispersion characteristics resemble those for Kelvin waves—at least for large vertical wavelengths ($m \ll N^2k^2/4N\beta$). For the westward-propagating waves, the dispersion curves depend weakly on both k and m, becoming nearly indistinguishable for $\tilde{k} > 4$.

The spectrum of the symmetric component of the meridional wind field in the lower stratosphere (Fig. 11) has a broad peak distributed approximately along the dispersion curve for westward-moving MRG waves with $L = 5$ km. Eastward-propagating features are found at small k along the $L = 5$ and $L = 15$ km dispersion curves, although these features have only ~10% of the power spectral density of the westward feature.

Latitude–frequency spectra for the $\tilde{k} = 4$ component of the meridional wind in the lower stratosphere (not shown) contain a westward-propagating symmetric peak with the meridional structure of an $L \approx 5$ km

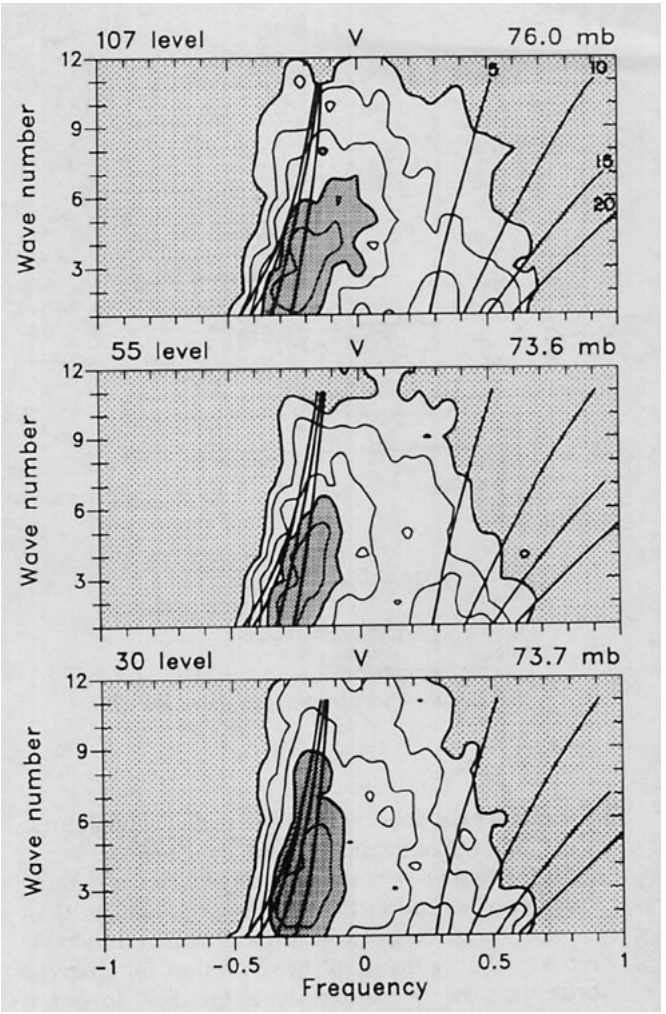

FIG. 11. As in Fig. 4, except that meridional wind power is shown near 75 mb and dispersion curves are shown for MRG waves with $L = \pm 5$, 10, 15, and 20 km.

MRG wave and a period $\approx$ 5 days ($\tilde{\omega} \approx 0.2$). This feature appears to correspond with the $\tilde{k} = 4$ MRG wave identified by Yanai and Maruyama (1966) and invoked in the QBO theory of Holton and Lindzen (1972).

Most of the observational evidence for the existence of the $\tilde{k} = 4$, $\tilde{\omega} \approx 0.2$ MRG wave comes from upper tropospheric and lower stratospheric rawinsonde observations over the western Pacific Ocean (see the review by Wallace 1971). However, this MRG wave is not a particularly strong feature in upper tropospheric wind spectra calculated from global analyses and may not always be present. For example, Yanai and Lu (1983) were able to identify this feature at 200 mb during June–August 1967 but not during June–August 1972. Randel (1992) has used a long series of ECMWF analyses to show that MRG waves occur intermittently at 200 mb. The L107 spectra in the upper troposphere (Fig. 12) agree reasonably well with the spectra computed by Randel from ECMWF analyses except for the

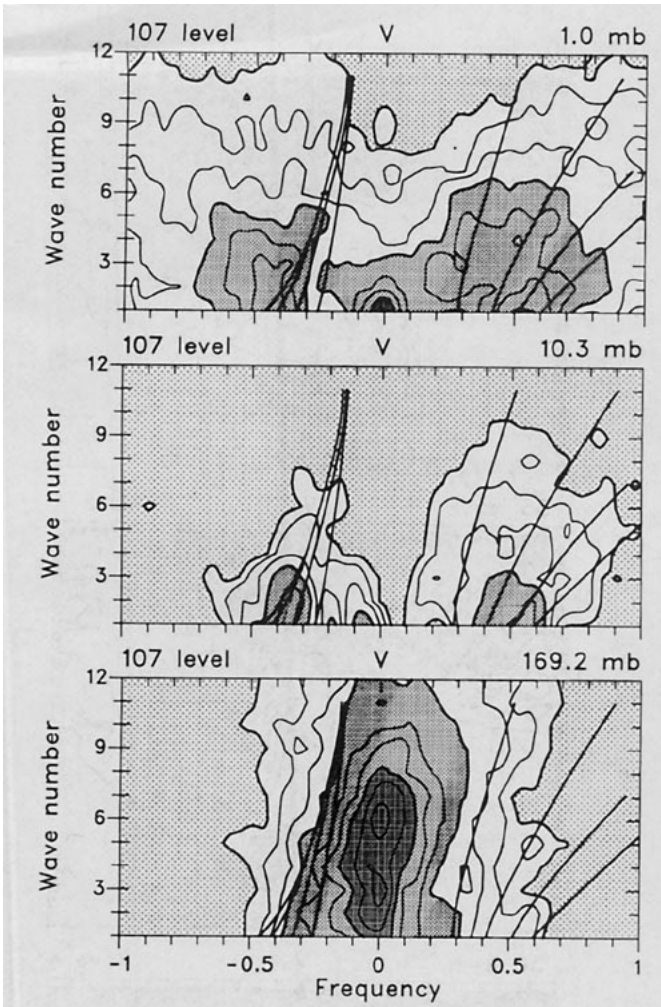

FIG. 12. As in Fig. 11, except that meridional wind power is shown for L107 near 1, 10, and 170 mb.

presence of a large amount of power near $\omega = 0$. This stationary power is found in all of the simulations and probably results from the presence of mean westerlies in the upper troposphere, allowing excessive penetration of midlatitude Rossby waves into the tropics.

The evolution of the wavenumber–frequency spectrum in the vertical is governed largely by the dependence of the vertical group velocity:

$$c_g^{(z)} = \frac{\mp\omega^3}{N(2\beta + \omega k)}, \qquad (4)$$

on frequency and zonal wavenumber. For eastward-moving waves, (4) resembles (2), the equivalent expression for Kelvin waves. Larger group velocities are found for larger k and L, so that power tends to shift both outward along dispersion curves and to the dispersion curves for larger L with increasing height. The shift to larger L can be seen in Figs. 11 and 12, where the maximum eastward power is found for $\tilde{k} = 1$ and $L = 5$ km in the lower stratosphere, with a secondary maximum for $\tilde{k} = 1$ and $L = 15$ km. At 10 mb and above, the $L = 15$ km dominates. This is the eastward MRG wave with period of about 2 days, which was discussed by Randel et al. (1990). It is more difficult to identify outward shifts of the power along dispersion curves, although there is some evidence of this for the $L = 15$ km feature between 10 and 1 mb.

The group velocity for westward-moving waves increases only with L and decreases with k. The effects of this dependence can be seen in Figs. 11 and 12, where the westward power shifts to higher frequency and lower k between 75 and 10 mb. At 10 mb, the maximum power lies between the $L = 10$ and $L \approx 15$ km dispersion curves, with period ~ 3 days. This wave was also discussed by Randel et al. (1990). The changes above 10 mb are complicated by the presence of additional (non-MRG) westward-moving waves in the spectrum. However, the MRG wave power continues to shift to higher frequency and longer vertical wavelength.

The fast eastward and westward MRG waves are striking features of the spectra for both temperature and meridional wind in the middle stratosphere when latitudinal distributions are examined (Fig. 13). There are symmetric peaks centered on the equator in the meridional wind spectrum near $\tilde{\omega} = -0.35$ and 0.5, corresponding to periods of 3 and 2 days, respectively. These peaks are associated with pairs of temperature peaks centered near 10° for the westward wave and near 15° for the eastward wave. The temperature power in these peaks is about 5% of that associated with the Kelvin waves. Further analysis has shown that the

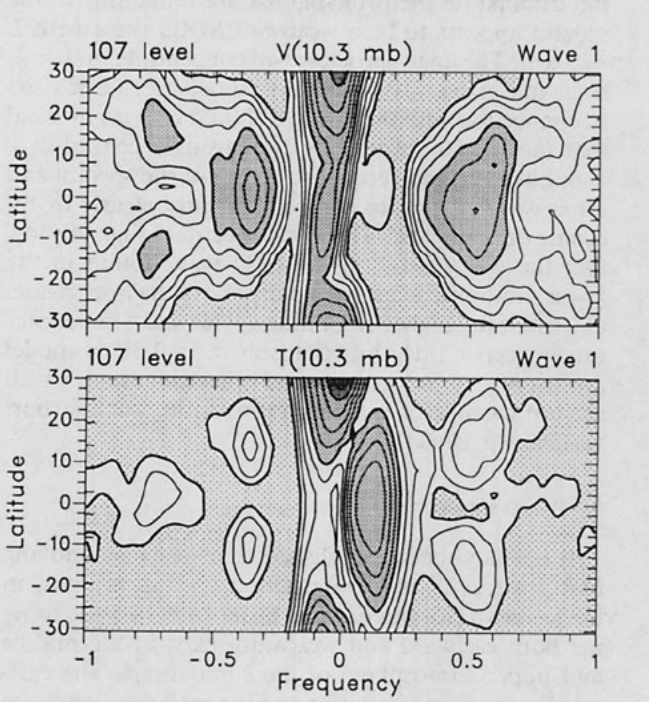

FIG. 13. As in Fig. 3, except that meridional wind and temperature power are shown for L107 near 10 mb.

temperature variations in these peaks are out of phase across the equator, as expected for MRG waves. The greater meridional extent of the eastward wave is in accordance with its longer vertical wavelength (~18 km as opposed to ~13 km). Similar behavior was found in observations by Randel et al. (1990).

At even higher frequencies in Fig. 13, small spectral maxima with the characteristics of inertio–gravity waves can be found. These waves have temperature perturbations symmetric about the equator and antisymmetric meridional wind perturbations, which result in paired peaks in the spectrum on either side of the equator. A westward-moving inertio–gravity wave with $\tilde{\omega} \approx -0.75$ (1.3-day period) is easily identifiable in Fig. 13. This wave has about one-half of the temperature power of the fast MRG waves and about one-third of the meridional wind power. An eastward-moving inertio–gravity wave with $\tilde{\omega} \approx 0.85$ can also be found in Fig. 13, but this wave is even weaker than the westward wave. These inertio–gravity waves do not appear to have any appreciable effect on the stratospheric circulation.

It is interesting that the westward-moving power in the lower stratosphere (~75 mb) emerges from a rather different spectrum in the upper troposphere (~170 mb). While there is some evidence that the 5-day westward MRG wave exists in the upper troposphere, it is a weak feature in the power spectra of both the model and the atmosphere. Spectra calculated from 200-mb global analyses by Randel (1992) maximize for slower frequencies (periods 6–10 days). Immediately above the tropopause the principal feature remaining in the spectra appears to be a westward MRG wave with $L \approx 5$ km. The analysis below will concentrate on $\tilde{k} = 4$, since this is the wave that has generally been discussed in connection with the QBO. It should be born in mind that the model spectra are not strongly peaked at $\tilde{k} = 4$; however, the vertical structure of the spectra and other wave properties can be seen most clearly by focusing on a single k. The $\tilde{k} = 4$ spectra in Fig. 14 show that the westward $L \approx 5$ MRG wave found in the lower stratosphere decays rapidly above the tropopause, at least at the higher resolutions. This wave penetrates much deeper into the stratosphere in L30, a model artifact related to the numerical approximations, which are not capable of properly representing such a short vertical wavelength.

b. *Wave structures*

It has now been established that westward-moving MRG waves of moderate period (~5 days) exist in the lower stratosphere, while faster MRG waves, moving both eastward and westward, exist in the middle and upper stratosphere of the simulations. The eastward-moving waves have periods near 2 days while the westward-moving waves have periods of 2–3 days, with period decreasing with height. The moderate westward-moving MRG wave is believed to be important in forcing the QBO, but its vertical wavelength ($L \approx 5$ km), as inferred from the dispersion relation, is so short that both the L30 and L55 simulations should have trouble resolving it. Five kilometers corresponds to three–four

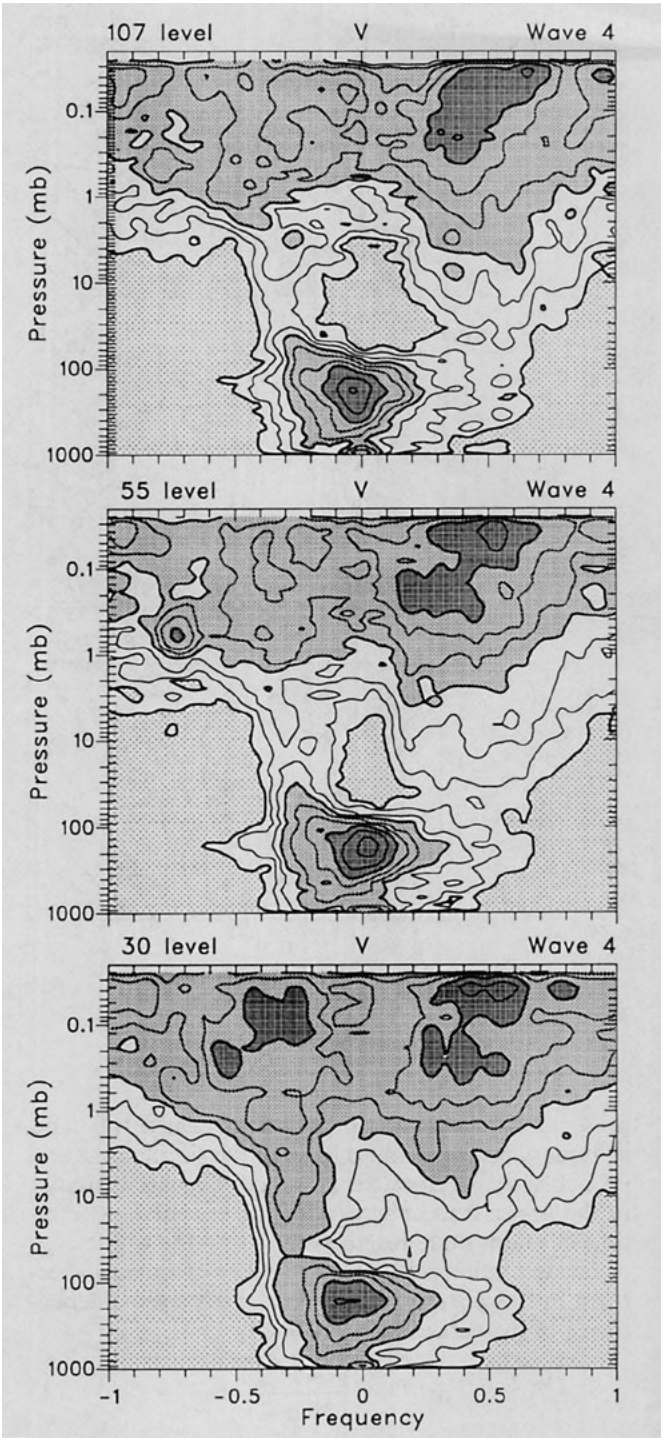

FIG. 14. Frequency–height cross sections of the $\tilde{k} = 4$ meridional wind power for L107, L55, and L30. Contours and stippling as in Fig. 3.

grid lengths in L55, while it is only about two grid lengths in L30. The faster waves are interesting because they exist in both the model and the atmosphere, but they do not appear to be significant in terms of affecting the circulation.

The $\tilde{k} = 4$ meridional amplitude, relative phase, and EP flux divergence are shown in Fig. 15 for the 5-day lower stratospheric westward MRG wave. Unfortunately, corresponding figures cannot be constructed from observations, even for amplitude and phase. For L107, the amplitude is nearly symmetric about the equator with $\sim 10°$ meridional scale. There is a small amount of asymmetry with larger values north of the equator, probably because of the horizontal shear in the mean zonal winds (Fig. 1). A coherent wave is found over a very limited region because of the rapid decrease of the amplitude with height. Immediately above the tropopause the amplitude is ~ 1 m s^{-1}, but the wave has vanished at 30 mb. In fact, a coherent oscillation is found over only a single vertical wavelength, as indicated by the phase lines.

The wavelength over the entire coherent region is ~ 6.5 km but decreases with height from ~ 8 km below 50 mb to ~ 5 km above 50 mb. The decrease in the vertical wavelength results from increasing zonal mean easterlies in the lower stratosphere, which decrease the intrinsic phase speed (and frequency). Over the region from 100 to 30 mb, the zonal mean wind at the equator decreases from near zero to ~ -10 m s^{-1}. The phase speed of the wave is -23 m s^{-1}, so that it has a critical level near 3 mb according to Fig. 1. Therefore, the absorption (vanishing) of the wave below 30 mb must be caused by processes other than critical-layer absorption. The shortening of the vertical wavelength as the easterlies strengthen increases the radiative damping rate and the effect of vertical diffusion on the wave, while the vertical group velocity decreases according to (4). All of these effects contribute to reducing the wave amplitude.

The wave structure varies considerably with resolution, as might be expected given the short vertical wavelengths involved. The L55 structure is surprisingly similar to the L107 structure, with a coherent oscillation found over about the same domain. The L55 amplitude also compares favorably with L107, although differences are readily apparent. However, L55 shows little evidence of the decrease in vertical wavelength with height found in L107. The L55 grid spacing is not adequate to permit significant reductions in the vertical wavelength. The L30 structure bears little resemblance to that at the higher resolutions. Although the L30 amplitude is similar to the L107 amplitude near 70 mb, the amplitude increases again above 50 mb (as was seen in the power spectra of Fig. 14), reaching a maximum near 20 mb. The entire region with coherent oscillations is shifted upward with respect to those for L107 and L55, with no coherent signal found below 100 mb. The meridional extent of the coherent signal is also reduced in L30 compared to the higher resolutions.

The structure of the fast westward (3-day period, $\tilde{k} = 1$) MRG wave mentioned above is shown in Fig. 16 for L107. This wave has a large enough vertical wavelength that its structure is similar at the lower resolutions. The vertical wavelength diagnosed from the dispersion curves in Fig. 12 was 10–15 km, which corresponds with $L \approx 10$ km determined from the phase lines in Fig. 16. A coherent wave is found over most of the stratosphere with maximum amplitude of 1.2 m s^{-1} near 3 mb. The amplitude of the fast MRG wave in the lower stratosphere is ~ 0.5 m s^{-1}, similar to that of the slower wave discussed above. There is northward shifting of the patterns in Fig. 16 above 10 mb, likely due to the mean wind shears (Fig. 2). A similar effect was found in observations by Randel et al. (1990; their Fig. 4a). Both the westward and eastward fast MRG wave identified here are also present in the simulation of Hayashi et al. (1984, see their Fig. 10), although not mentioned in the text of that paper.

c. *Wave forcing of mean flow*

The EP flux divergence associated with the moderate westward MRG wave is confined to a small region above the tropopause, corresponding with the rapid decay of the wave amplitude. The maximum EP flux divergence for L107 is ~ 0.01 m s^{-1}/day, similar to that produced by the slow Kelvin wave, although the MRG wave maximum occurs somewhat lower. Since the MRG wave spectrum is not as strongly peaked as the Kelvin wave spectrum, the net easterly forcing produced by MRG waves of moderate phase speed in L107 is somewhat larger than the westerly forcing produced by slow Kelvin waves. However, this forcing is still an order of magnitude smaller than would be required in order to produce a realistic QBO. The MRG wave forcing is also confined much too low in the stratosphere. For the zonal winds found in L107, QBO models based on Holton and Lindzen (1972) would have maximum easterly forcing immediately below the critical level near 3 mb.

The variation of the simulated EP flux divergence with vertical resolution is substantial. The L30 EP flux divergence is less than half of that in L107. As with the amplitudes, L55 is surprisingly similar to L107. Some of the vertical structure seen in L107 is not found in L55, but the magnitude of the EP flux divergence is nearly the same. The biggest difference between L107 and L55 is that L55 EP flux divergence is nearly symmetric about the equator. The maximum EP flux divergence in L107 shifts from south of the equator immediately above the tropopause to symmetric about the equator slightly higher up.

The EP flux divergence for the fast westward MRG wave is not shown because it is negligible at all levels. This is also true for the fast eastward MRG wave.

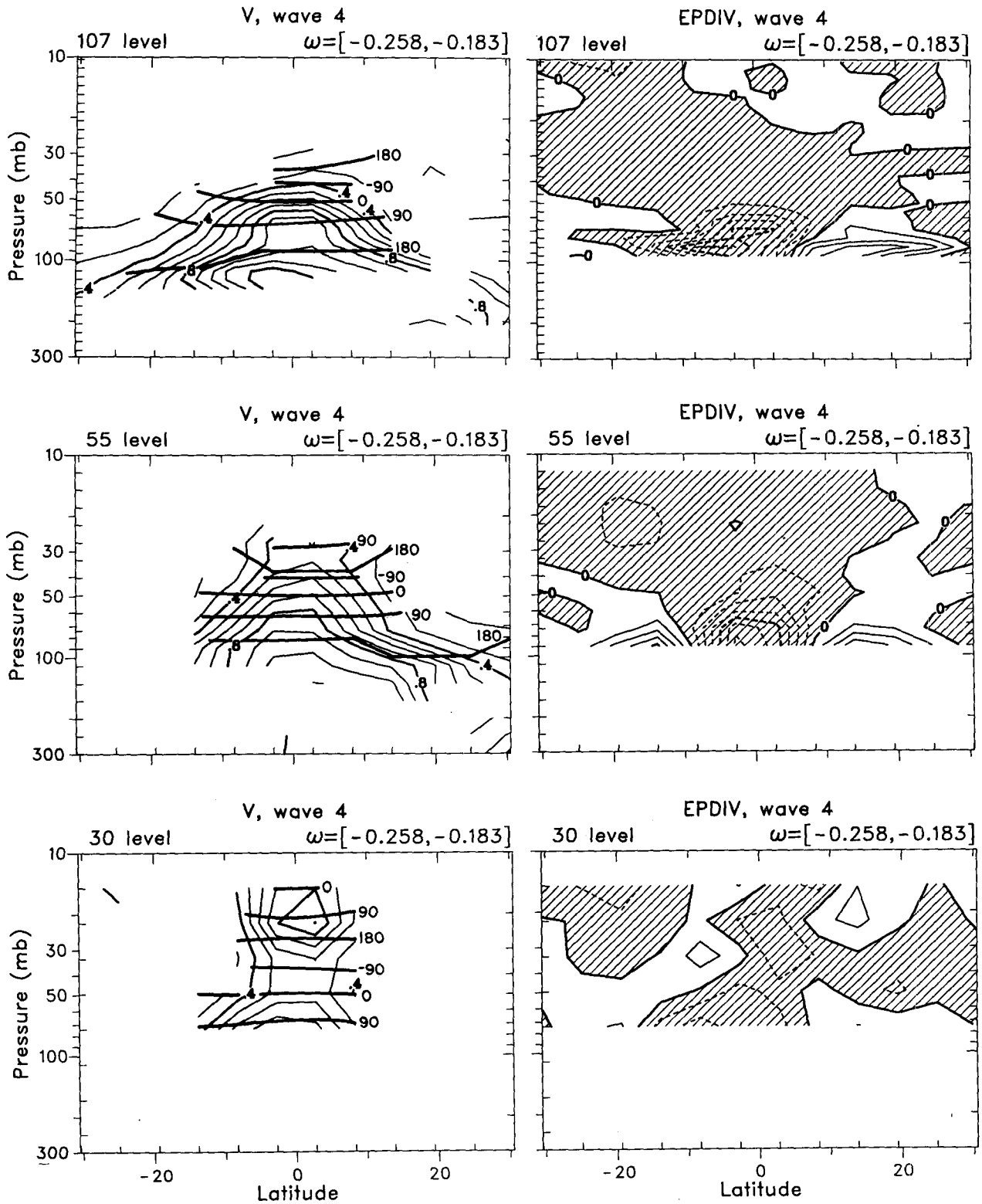

FIG. 15. As in Fig. 6, except that meridional wind is shown in place of temperature. The center of the frequency band corresponds to a period of 5 days, the reference point for phase is at 50 mb and 2.2°S, and the contour intervals are 0.1 m s^{-1} for meridional wind and 2 $\times 10^{-3}$ m s^{-1}/day for EP flux divergence.

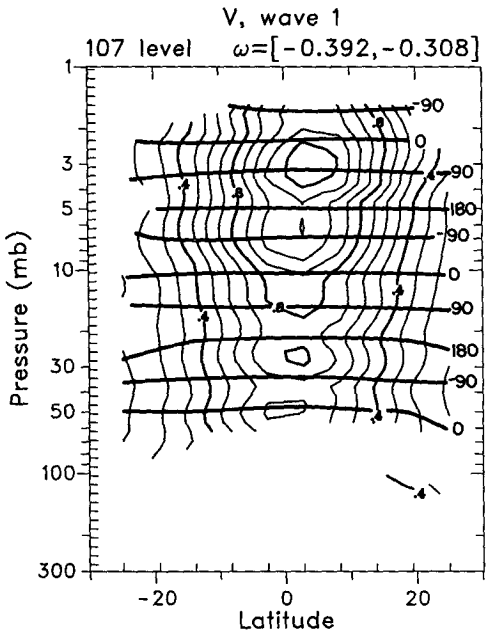

FIG. 16. As in Fig. 15, except that only the meridional wind for L107 is shown. The center of the frequency band corresponds to a period of 3 days, and the reference point for phase is at 10 mb and 2.2°S.

5. Conclusions

The GCM simulations examined here contain several classes of equatorially trapped waves, including Kelvin, MRG, and inertio–gravity waves. The particular examples of these waves found in the model are characterized by the range of vertical wavelengths between 5 and 20 km. There does not appear to be a continuous distribution of waves; instead discrete wave groups of each class are found that have wavenumbers and frequencies distributed along the dispersion curves for particular vertical wavelengths. The 15-day, $\tilde{k} = 1$ Kelvin wave and the 5-day, $\tilde{k} = 4$ MRG wave believed to be important in forcing the QBO are found in the simulations.

Only limited observations of the equatorial stratosphere are available, rendering detailed verifications of the simulated wave properties impossible. Kelvin waves are most readily identifiable in satellite temperature observations, and the 15- and 7.5-day modes found in the model results compare reasonably well with LIMS data. The faster 4-day wave in LIMS data is not found here but is not apparent every year in observations either, according to Randel and Gille (1991). Randel et al. (1990) used the model simulations to identify planetary-scale MRG waves in LIMS observations of the upper stratosphere. Only the fast inertio–gravity waves have not as yet been identified in an observational dataset. These waves have no apparent importance other than as "naturally" occurring examples of waves that are well known to be theoretically possible solutions of the primitive equations.

Theoretical and simplified modeling studies have indicated that the forcing depth should be the primary factor determining the vertical wavelength (and frequency through the dispersion relation) of equatorial waves. This expectation is consistent with the range of

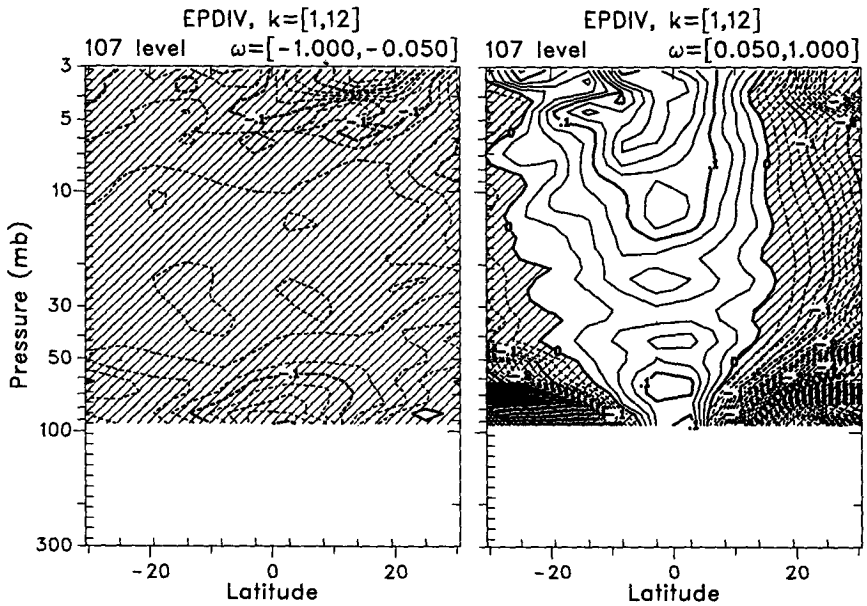

FIG. 17. Latitude–height cross sections of the L107 total EP flux divergence for waves 1–12 summed over all westward (left) and eastward frequencies (right) faster than 20 days^{-1}. The contour interval is 0.025 m s^{-1}/day; negative contours are dashed.

vertical wavelengths (5–20 km) for which equatorial waves are found in the current simulations. It is also interesting that there is little evidence below the tropopause of either the Kelvin or MRG waves that dominate the power spectra in the lower stratosphere. The spectral peaks associated with these waves emerge immediately above the tropopause from tropospheric spectra with completely different temporal and spatial characteristics. The MRG waves in the lower stratosphere have shorter vertical wavelengths (5–8 km) than do the Kelvin waves (10–15 km). This suggests that the forcing of the MRG waves may be different than that for the Kelvin waves. In this context, it is interesting to note that Salby and Garcia (1987) were able to produce Kelvin waves but not MRG waves using stochastic thermal forcing.

The Kelvin and MRG waves, believed to be important in forcing the QBO, have relatively short vertical wavelengths (5–10 km). Consequently, the characteristics of these waves change substantially with vertical resolution between simulations with 2.8-, 1.4-, and 0.7-km grid spacings. However, the wave properties change much less between the 1.4- and 0.7-km resolutions than between the 2.8- and 1.4-km resolutions. In fact, the forcing of the mean flow by the equatorial waves is similar at the two higher resolutions. It appears that vertical resolution of about 1 km should be adequate to simulate the waves believed to force the QBO.

The vertical resolutions used in the simulations discussed here are all greater than could be justified using quasigeostrophic scaling arguments appropriate to the extratropical regime. A model designed to simulate the extratropics would require horizontal resolution of about 100 km in order to justify 1-km vertical resolution. Only the GFDL SKYHI model has been used for stratospheric simulations with horizontal resolution near 100 km (Mahlman and Umscheid 1987). However, the vertical resolution of that model was not adjusted to maintain compatibility with the horizontal resolution. As has been common with other studies varying the horizontal resolution of models (e.g., Boville 1991), Mahlman and Umscheid (1987) held the vertical resolution fixed (at about 1.7 km in the lower stratosphere) while increasing the horizontal resolution.

The magnitudes of the Kelvin and MRG waves produced by the high-resolution simulations were comparable to the observed values. However, the zonal momentum forcing (EP flux divergence) produced by these waves in the lower stratosphere was at most 10% of the forcing required to explain the observed QBO accelerations. The result is more encouraging when the EP flux divergence is integrated over zonal wavenumber and eastward or westward frequencies, as shown in Fig. 17. The total forcing by both eastward and westward waves is approximately symmetric about the equator in the lower stratosphere and is about 10 times bigger than the EP flux divergence associated with the single waves discussed above. Thus, the forcing of the mean flow by the waves is comparable to the mean-flow acceleration observed in the QBO. However, the results of Takahashi and Boville (1991) indicate that EP flux divergences of ~ 0.4 m s^{-1}/day are required to produce a realistic QBO in a three-dimensional model.

In summary, the simulated equatorial wave modes are as large as the observed modes, and the simulated wave spectra agree with the observed spectra to the extent that the latter can be determined. In spite of this agreement, the total wave driving produced by the model is too small to force a QBO. This fact has recently been verified by a multiyear integration with 1-km vertical resolution. Either the shape of the model's equatorial wave spectrum differs from reality outside of the small range sampled by observations or additional processes, such as gravity waves, must be important in forcing the QBO in the atmosphere.

Acknowledgments. The authors wish to thank Drs. Masaaki Takahashi and Rolando Garcia for many fruitful discussions. This work was partially supported by the NASA Upper Atmosphere Theory and Analysis Program under Order W-16,215.

REFERENCES

Andrews, D. G., J. R. Holton, and C. B. Leovy, 1987: *Middle Atmosphere Dynamics.* Academic Press, 489 pp.

Belmont, A. D., D. G. Dartt, and G. D. Nastrom, 1975: Variations of stratospheric zonal winds, 20–65 km, 1961–1971. *J. Appl. Meteor.,* **14,** 585–594.

Boville, B. A., 1991: Sensitivity of simulated climate to model resolution. *J. Climate,* **4,** 469–485.

——, and W. J. Randel, 1986: Observations and simulation of the variability of the stratosphere and troposphere in January. *J. Atmos. Sci.,* **43,** 3015–3034.

——, and X. Cheng, 1988: Upper boundary effects in a general circulation model. *J. Atmos. Sci.,* **45,** 2592–2606.

——, and D. P. Baumhefner, 1990: Simulated forecast error and climate drift resulting from the omission of the upper stratosphere in numerical models. *Mon. Wea. Rev.,* **118,** 1517–1530.

Delisi, D. P., and T. J. Dunkerton, 1988: Seasonal variation of the semiannual oscillation. *J. Atmos. Sci.,* **45,** 2772–2787.

Dunkerton, T. J., 1981: Wave transience in a compressible atmosphere. Part II: Transient equatorial waves in the quasi-biennial oscillation. *J. Atmos. Sci.,* **38,** 298–307.

——, C.-P. F. Hsu, and M. E. McIntyre, 1981: Some Eulerian and Lagrangian diagnostics for a model stratospheric warming. *J. Atmos. Sci.,* **38,** 819–843.

Fels, S. B., 1982: A parameterization of scale-dependent radiative damping rates in the middle atmosphere. *J. Atmos. Sci.,* **39,** 1141–1152.

Gille, J. C., and J. M. Russell, 1984: The limb infrared monitor of the stratosphere: Experiment description, performance, and results. *J. Geophys. Res.,* **89,** 5125–5140.

——, ——, P. L. Bailey, L. L. Gordley, E. E. Remsberg, J. H. Lienesch, W. G. Planet, F. B. House, L. V. Lyjak, and S. A. Beck, 1984: Validation of temperature retrievals obtained by the limb infrared monitor of the stratosphere (LIMS) experiment on *Nimbus 7. J. Geophys. Res.,* **89,** 5147–5160.

Hamilton, K., and J. D. Mahlman, 1988: General circulation model simulation of the semiannual oscillation of the tropical middle atmosphere. *J. Atmos. Sci.,* **45,** 3212–3235.

Hayashi, Y., D. Golder, and J. D. Mahlman, 1984: Stratospheric

and mesospheric Kelvin waves simulated by the GFDL "SKYHI" general circulation model. *J. Atmos. Sci.*, **41**, 1971–1984.

Hitchman, M. H., and C. B. Leovy, 1986: Evolution of the zonal mean state in the equatorial middle atmosphere during October 1978–May 1979. *J. Atmos. Sci.*, **43**, 3159–3176.

Holton, J. R., and R. S. Lindzen, 1972: An updated theory for the quasi-biennial cycle of the tropical stratosphere. *J. Atmos. Sci.*, **29**, 1076–1080.

Lindzen, R. S., and J. R. Holton, 1968: A theory of the quasi-biennial oscillation. *J. Atmos. Sci.*, **25**, 1095–1107.

Mahlman, J. D., and L. J. Umscheid, 1984: Dynamics of the middle atmosphere: Successes and problems of the GFDL "SKYHI" general circulation model. *Dynamics of the Middle Atmosphere*, J. R. Holton and T. Matsuno, Eds., Terra Scientific, 501–526.

——, and ——, 1987: Comprehensive modeling of the middle atmosphere: The influence of resolution. *Transport Processes in the Middle Atmosphere*, G. Visconti and R. Garcia, Eds., D. Reidel, 251–266.

Naujokat, B., 1986: An update of the observed quasi-biennial oscillation of the stratospheric winds over the tropics. *J. Atmos. Sci.*, **43**, 1873–1877.

Plumb, R. A., 1984: The quasi-biennial oscillation. *Dynamics of the Middle Atmosphere*, J. R. Holton and T. Matsuno, Eds., Terra Scientific, 217–251.

——, and R. C. Bell, 1982: A model of the quasi-biennial oscillation on an equatorial beta-plane. *Quart. J. Roy. Meteor. Soc.*, **108**, 335–352.

Randel, W. J., 1992: Upper tropospheric equatorial waves in ECMWF analyses. *Quart. J. Roy. Meteor. Soc.*, in press.

——, and J. C. Gille, 1991: Kelvin wave variability in the upper stratosphere observed in SBUV ozone data. *J. Atmos. Sci.*, **48**, 2336–2349.

——, B. A. Boville, and J. C. Gille, 1990: Observations of planetary mixed Rossby-gravity waves in the upper stratosphere. *J. Atmos. Sci.*, **47**, 3092–3099.

Reed, R. J., W. J. Campbell, L. A. Rasmusson, and D. C. Rogers, 1961: Evidence of the downward-propagating annual wind reversal in the equatorial stratosphere. *J. Geophys. Res.*, **66**, 813–818.

Rind, D., R. Suozzo, N. K. Balachandran, A. Lacis, and G. Russell, 1988a: The GISS global climate—middle atmosphere model. Part I: Model structure and climatology. *J. Atmos. Sci.*, **45**, 329–370.

——, ——, and ——, 1988b: The GISS global climate—middle atmosphere model. Part II: Model variability due to interactions between planetary waves, the mean circulation and gravity wave drag. *J. Atmos. Sci.*, **45**, 371–386.

Salby, M. L., and R. R. Garcia, 1987: Transient response to localized episodic heating in the tropics. Part I: Excitation and short-time near-field behavior. *J. Atmos. Sci.*, **44**, 458–498.

——, D. L. Hartmann, P. L. Bailey, and J. C. Gille, 1984: Evidence for equatorial Kelvin waves in *Nimbus-7* LIMS. *J. Atmos. Sci.*, **41**, 220–235.

Simmons, A. J., and R. Strüfing, 1983: Numerical forecasts of stratospheric warming events using a model with a hybrid vertical coordinate. *Quart. J. Roy. Meteor. Soc.*, **109**, 81–111.

Takahashi, M., 1987: A two-dimensional numerical model of the quasi-biennial oscillation: Part I. *J. Meteor. Soc. Japan*, **65**, 523–536.

——, and B. A. Boville, 1992: A three-dimensional simulation of the equatorial quasi-biennial oscillation. *J. Atmos. Sci.*, in press.

Veryard, R. G., and R. A. Ebdon, 1961: Fluctuations in tropical stratospheric winds. *Meteor. Mag.*, **90**, 125–143.

Wallace, J. M., 1971: Spectral studies of tropospheric wave disturbances in the tropical western Pacific. *Revs. Geophys. Space Phys.*, **9**, 333–349.

——, and V. E. Kousky, 1968: Observational evidence of Kelvin waves in the tropical stratosphere. *J. Atmos. Sci.*, **25**, 900–907.

Williamson, D. L., J. T. Kiehl, V. Ramanathan, R. E. Dickinson, and J. J. Hack, 1987: Description of NCAR Community Climate Model (CCM1). NCAR Tech. Note, NCAR/TN-285+STR, 112 pp. [Available from National Center for Atmospheric Research, Boulder, CO; NTIS PB87-203782/AS].

Yanai, M., and T. Maruyama, 1966: Stratospheric wave disturbances propagating over the equatorial Pacific. *J. Meteor. Soc. Japan*, **44**, 289–294.

——, and M.-M. Lu, 1983: Equatorially trapped waves at the 200-mb level and their association with meridional convergence of wave energy flux. *J. Atmos. Sci.*, **40**, 2785–2803.